Asian Journal of Chemistry; Vol. 35, No. 4 (2023), 851-860

ASIAN JOURNAL OF CHEMISTRY

https://doi.org/10.14233/ajchem.2023.27290

Enhancing Corrosion Resistance Property of Mild Steel by Benzoxazine Synthesized from Vanillin and Copolymerize with Urethane

K. JAYANTHI[1,*], M. SIVARAJU[2] and P. SHANMUGASUNDARAM[2]

[1]P.G. and Research Department of Chemistry, Queen Mary's College (A), Chennai-600004, India
[2]P.G. and Research Department of Chemistry, Thiruvalluvar Government Arts College, Rasipuram-637401, India

*Corresponding author: E-mail: kjayanthi_che@queenmaryscollege.edu.in

Received: 12 December 2022; *Accepted*: 27 January 2023; *Published online*: 30 March 2023; AJC-21181

Benzoxazine monomer prepared from vanillin and *n*-butylamine was characterized by ^{1}H NMR, ^{13}C NMR, FT-IR and UV visible spectroscopic techniques. The synthesized monomer was coated on the mild steel with isocyanate hardener in varying concentrations of isocyanate of the poly(VaBz-PU) and cured. The thermal properties of the monomer with and without isocyanate hardener were studied by TGA and DSC methods. The effect of various concentrations of isocyanate (PU) hardener with benzoxazine monomer on hardness, water absorption and gel absorption was investigated. Various concentrations of PU hardener with benzoxazine coating (VaBz-PU) on the mild steel were investigated by the electrochemical impedance and polarization studies. The study revealed that an increasing concentration of isocyante in the coating with benzoxazine increased their thermal, chemical and anticorrosive properties. The DFT calculations were also performed to support the anti-corrosive ability of the material.

Keywords: Benzoxazine, Vanillin, Polyurethane copolymer, Electrochemical impedance, Corrosion, Polarization.

INTRODUCTION

Mild steel is a type of low carbon steel having ductile, excellent mechanical properties, can be carburized, recyclable, *etc.* and has been widely used in many industries due to its cost effectiveness [1]. Some industrial practices use mild steel in sodium chloride medium and get extremely affected by corrosion including the corrosion of the food cans, pipes buried into the ground, ships, bridges and oil pipelines due to the high salinity of the water. During some chemical industrial processes like cleaning, pickling, descaling or sometimes with transportation mild steel may be corroded by NaCl solution [2-4]. When NaCl solution comes into contact with marine environments, corrosion occurs in pipelines that cross or are close to salt water. The dissolution of iron due to the presence of NaCl is considered as one of the main reasons for the occurrence of corrosion of these materials. In order to reduce the corrosion rate, inhibition and protection of the metal will result in the following development of methods and materials [5-9].

Inhibitors are defined as low concentration of substances or mixture substances used in the corrosion environment to inhibit, prevent or minimize the corrosion rate [10]. Many organic compounds containing nitrogen, oxygen and sulphur atoms (heterocyclic compounds) and plant extract can also be used as inhibitor. Nowadays, polybenzoxazine along with urethane coating are also used as a new class of novel corrosion inhibitors, because of their low water absorption, good hydrophobicity, near zero shrinkage and good dielectric properties [11,12]. Polybenzoxazine is a thermosetting phenolic resin, which exhibits desirable properties like chemical resistance and thermal stability, high char yield, long shelf life, and flame resistance. Benzoxazine monomers can be easily synthesized by Mannich condensation reaction [13]. Zhou *et al.* [14] showed that polybenzoxazine/epoxide composite coatings perform good corrosion resistance with a high charge-transfer resistance. Due to the disrupting nature of bisphenol-A (BPA) on natural hormones, replacement of BPA introduces many non-disrupting starting materials. Pollution-free bio-based bisguaiacol-F based benzoxazines [15]. Guaiacol based benzoxazine monomers and cardanol based benzoxazine monomers were reported to have anticorrosive properties [16,17]. In recent times, petroleum based raw materials is becoming a major environmental issue,

like waste disposal and depletion of petroleum resources, the need for alternative materials is vital. Polybenzoxazine has been synthesized from a range of renewable phenols such as vanillin [18-21]. Eugenol/stearylamine-based benzoxazine and pyrogallol/furfurylamine-based benzoxazine from bio-based raw material [22].

Eugenol based polyols for the anticorrosive polyurethane coatings showed excellent anti-corrosive performance as analyzed by immersion and electrochemical methods against aq. 3.5% NaCl solution [23]. Several commercial isocyanates, and as polyols have the pre-eminent role in the determination of polyurethane properties, synthesis of polyol should be carefully evaluated, because their application in coating, adhesive and foams are dependent upon the hydroxyl value and chemical structure of polyols [24-28].

Based on the literature reviews and the high anti-corrosive nature of the polybenzoxazine/urethane coating on the metal surface, benzoxazine based monomer was synthesized from vanillin, butylamine by Mannich condensation method and copolymerized with urethane hardener during coating. Their applications on the corrosion resistance property on mild steel surface in 3.5% NaCl medium, thermal stability by TGA and DSC methods were studied. Density functional theory (DFT) studies of monomers were also performed to support the corrosion results.

EXPERIMENTAL

Thermo Scientific Nicolet iS50 FT-IR spectrometer was used for recording the FT-IR spectra. The Labman LMSP UV-1200 UV-Vis spectrometer was used for recording the UV-Vis spectrum, ^{1}H NMR and ^{13}C NMR spectra were recorded on Bruker 500 MHz and 125 MHz instruments in DMSO-d_6 for proton and carbon spectra, respectively. The progress and completion of reactions was checked by TLC on 2 × 5 cm pre-coated silica gel 60 F_{254} plates of a thickness of 0.25 mm (Merck). The TLCs were visualized under UV 254-365 nm and/or iodine. Polarization measurements were carried out in a conventional three-electrode cell. The Ag/AgCl and the platinum electrode were used as reference and counter electrodes, respectively. The potentiostatic polarization measurement was carried out using the Electrochemical workstation Biologic SP 300 model. The thermogravimetric analysis (TGA) of coating was performed using Pyris-1-TGA Perkin-Elmer thermogravimetric analyzer (Temperature range: 0-800 ºC). The surface analysis was performed on a JEOL JSM 6390 scanning electron microscope, where the acceleration beam energy was employed at 20 keV.

Synthesis of 3-butyl-8-methoxy-3,4-dihydro-2*H*-benzo-[*e*][1,3]oxazine-6-carbaldehyde (VaBz): Vanillin (1g, 6.572 mmol), *n*-butylamine (0.653 mL, 6.572 mmol) and paraformaldehyde (0.414 g, 13.802) were dissolved in toluene (20 mL) and refluxed for 24 h. The completion of the reaction was monitored by thin layer chromatography. After completion of the reaction, the reaction mixture was extracted with ethyl acetate (150 mL) and then washed with 1 N NaOH solution (2 × 100 mL), water (100 mL) and brine solution (100 mL). The organic layer was separated and dried over an anhydrous sodium sulphate solution. The evaporation of solvent yielded VaBz (**Scheme-I**). ^{1}H NMR (500 MHz, DMSO-d_6) ppm: 9.82 (1H, s), 7.32 (2H, s), 5.03 (2H, s), 4.07 (2H, s), 3.85 (3H, s), 2.67 (2H, t), 1.54- 1.50 (2H, m), 1.36-1.31 (2H, m), 0.94 (3H, t); ^{13}C NMR (125 MHz, DMSO-d_6) ppm: 191.78, 149.76, 148.34, 128.73, 124.53, 121.17, 108.93, 83.66, 55.96, 50.72, 49.15, 29.95, 20.21, 14.27. UV-Vis λ_{max}: 275, 302 nm. FT-IR (ν_{max}, KBr, cm^{-1}): 2946, 1685, 1591, 1500, 1444, 1279, 1143, 1073, 864.

Synthesis of VaBz-PU copolymer by dip coating: MS substrates were mechanically blasted to Sa 2.1/2 and cleaned ultrasonically in acetone before coating. The polymer was coated on the MS plate using dip coating and thermal curing methods. The monomer (Bz) was first dissolved in a mixture of solvents (7:3 1,4-dioxane/toluene) and then various equivalent amounts of the isocyanate hardener were added to that, such as 100:60 (Bz-PU 60), 100:80 (Bz-PU 80) and 100:100 (Bz-PU 100). The MS plate was then dipped in the Bz solution for 1 min and removed from it at a speed of 100 mm/min. Following three iterations of this procedure, Bz-coated MS samples were dried in a vacuum for 1 h at 100 ºC in order to eliminate the solvent, after being left at room temperature overnight. Finally, this specimen was then thermally treated for 3 h at 180 ºC.

Water absorption: Water absorption of cured coating samples were performed as per ASTM D570. The cured coating samples were dried at 80 ºC in a vacuum oven and then immersed in water for 24 h at room temperature. The cured samples were removed from water, then blotted with tissue paper and weighed. The percentage water absorption was calculated by eqn. 1:

$$\text{Water absorption} = \frac{W_a - W_b}{W_b} \times 100 \quad (1)$$

where W_a = Weight of the cured sample after removal the exposure to water absorption; W_b = Weight of the cured sample before removal the exposure to water absorption.

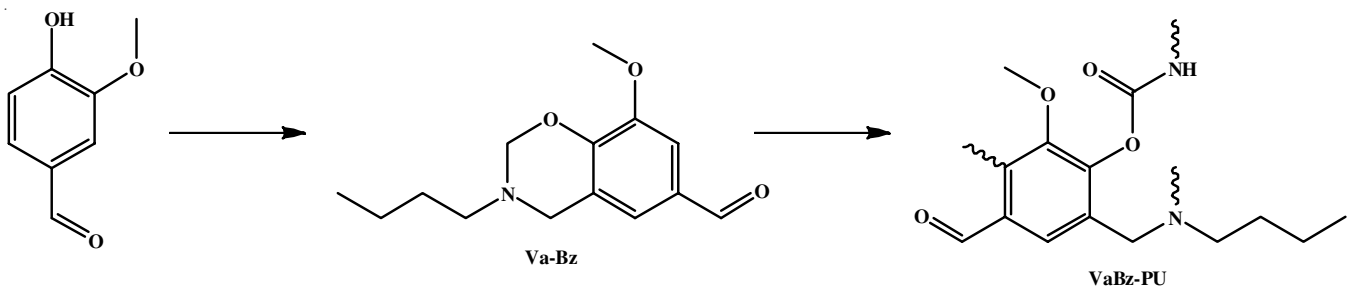

Scheme-I: Synthetic representation of monomer and polymer formation

Gel content: The gel content of cured coating sample was determined by weighing the cured sample accurately and extracted in xylene for 24 h at room temperature. Then the cured coating samples were dried in the oven. The gel content of the coating was calculated by eqn. 2:

$$\text{Gel absorption} = \frac{W_a}{W_b} \times 100 \quad (2)$$

where W_a and W_b are the weight of cured coating samples after and before the extraction, respectively.

Microhardness: Microhardness of compressed specimens was measured utilizing a Vickers microhardness tester (Tester MH6) The loading load during the test is 200 g to 262.1 g and the loading time is 10 s.

DFT studies: All the computational calculations including representation of HOMO and LUMO in the checkpoint files was developed with the Gaussian 09W program using density functional theory. The chemical structure of the Va-Bz was optimized with the B3LYP/6.31 G basis set. The Gauss view software package was used to visualize the computed structures including HOMO, LUMO and molecular electrostatic potential (MEP) representations.

RESULTS AND DISCUSSION

The Mannich reaction of vanillin with *n*-butylamine and paraformaldehyde in toluene medium yielded the Va-Bz (**Scheme-II**). The synthesized Va-Bz was characterized by ^{1}H NMR, ^{13}C NMR, FT-IR and UV-visible spectroscopic techniques. The Va-Bz is cured with various ratios of polyurethane. The monomer and polymers are also characterized by FT-IR and UV-visible spectroscopic techniques.

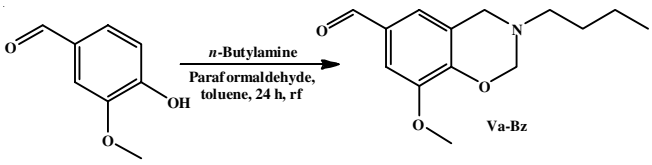

Scheme-II: Synthetic route of Va-Bz

IR studies: The FTIR vibrational frequencies of the Va-Bz and three different Bz-PUs are given in Table-1. The band appears at 864 cm^{-1} shows that the formation of a benzoxazine ring and the band appears at the1679 to 1685 cm^{-1} shows that the aromatic aldehyde -C=O stretching, asymmetric C-O stretching band appears at 1279 and 1290 cm^{-1}, N-C stretching band appears at 1143 cm^{-1}, symmetric O-C stretching band appears at 1073 cm^{-1}. The FT-IR spectrum of VaBz and Bz:PU are represented in Fig. 1.

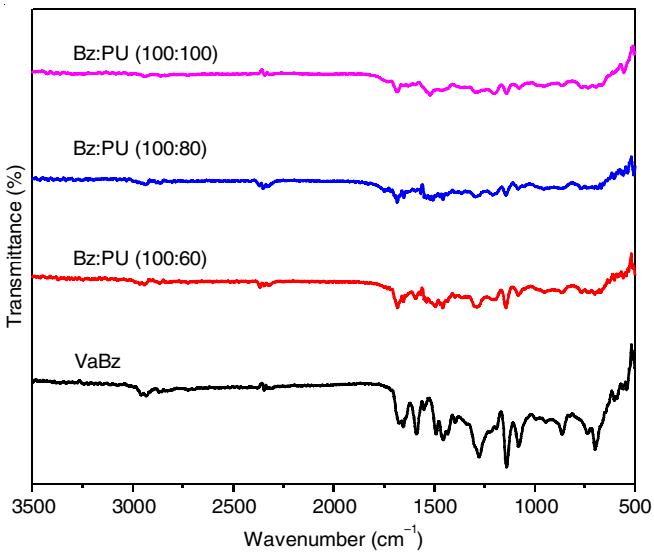

Fig. 1. FT-IR spectrum of VaBz monomer and different Bz-PU copolymer

^{1}H NMR spectrum of monomer: The ^{1}H NMR spectrum clearly showed the signals for 19 protons. The triplet appear at 0.94 ppm for 3 protons represents the methyl protons signal of the *n*-butyl unit, the multiplet in the range of 1.36-1.31 ppm for 2 protons, multiplet in the range of 1.54-1.50 ppm for 2 protons and triplet at 2.67 ppm are appeared for *n*-butyl alkyl protons. The methoxy protons appeared as singlet at 3.85 ppm. The benzoxazine CH_2 protons appeared as singlet at 4.07 and 5.03 ppm, respectively. The aromatic protons signal for 2 protons appear at 7.32 ppm. The appearance of a sharp singlet at 9.82 ppm for one proton indicates the presence of an aldehyde unit.

^{13}C NMR spectrum of monomer: The ^{13}C NMR showed the 14 carbon signals. The carbon signal appearing at 14.27, 20.21, 29.95 and 49.15 ppm indicates the presence of *n*-butyl units. The methoxy carbon appeared at 50.72 ppm. The benzoxazine CH_2 carbons appeared at 55.96 and 83.66 ppm, respectively. The aldehyde carbon appeared at the downfield region exactly appeared at 191.78 ppm, while the remaining aryl carbons appear at 149.76, 148.34, 128.73, 124.53 and 108.93 ppm correspondingly.

UV-Vis studies of VaBz monomer and different VaBzPU copolymers: Two absorption bands were found in the UV-visible spectrum of VaBz at 275 and 302 nm, respectively.

TABLE-1
INFRARED (cm^{-1}) SPECTRAL ASSIGNMENTS OF VaBz, Bz:PU (100:60), Bz:PU (100:80) AND Bz:PU (100:100)

Benzoxazine	Bz:PU (100:60)	Bz:PU (100:80)	Bz:PU (100:100)	Assignment
2946	2946	2946	2946	C-H stretching
1685	1679	1679	1679	Aromatic C=O stretch [29]
1591	1591	1591	1591	Aromatic C=C
1500	1500	1500	1500	
1279	1290	1290	1290	Asymmetric C-O-C stretching band
1143	1143	1143	1143	N-C stretching band
1073	1073	1073	1073	Symmetric O-C stretching band
864	864	864	864	Benzoxazine related band [30]

The absorbance appeared is due to π–π* and n–π* transition of VaBz. The addition of polyurethane in the VaBz shifted their absorbance to the red-shift region. The absorbance of VaBz:PUs is identified as 280 and 307 nm, respectively. The absorbance at 307 nm corresponds to the low energy intramolecular charge transfer (ICT) π–π* transition and which is coherent with previous benzoxazine reports [31-33]. The UV-visible spectrum of VaBz and Bz:PUs is represented in Fig. 2.

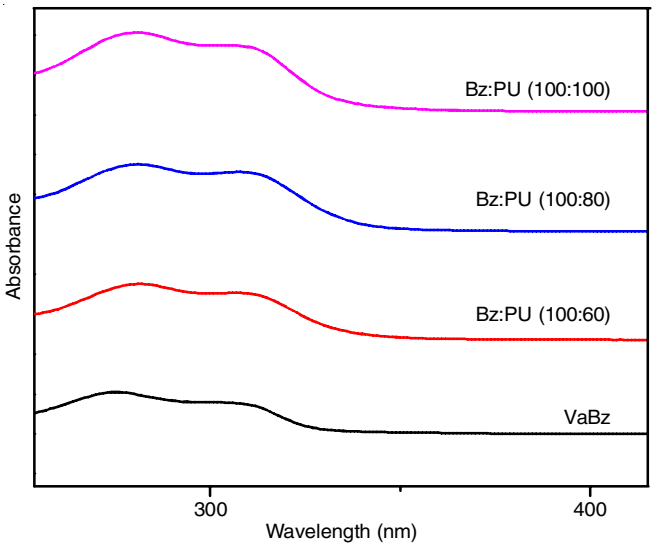

Fig. 2. UV-Vis spectrum of VaBz and Bz:PUsm

Corrosion studies

Potentiostatic polarization measurements: Polarization measurements were carried out in a conventional three-electrode cell. Mild steel strips coated with VaBz, VaBz with different concentrations of isocyanate hardener such as Bz:PU, 100:60, 100:80 and 100:100 only on the exposed area of 1 cm^2 were used as the working electrode. The corrosion resistance of VaBz and BzPU coatings on mild steel was investigated by the Tafel extrapolation method. Tafel polarization curves obtained with samples are shown in Fig. 3, from which the corrosion current (I_{corr}) and corrosion potential (E_{corr}) were calculated. The corrosion current density was determined by superimposing a straight line along the linear portion of the cathodic or anodic curve and extrapolating it through corrosion potential [34]. The more negative E_{corr} and the larger I_{corr} usually correspond to a faster corrosion rate while more positive E_{corr} and smaller I_{corr} mean a slower corrosion process [35]. The corrosion rate and protection efficiency (E) was calculated by using eqns. 3 and 4, respectively:

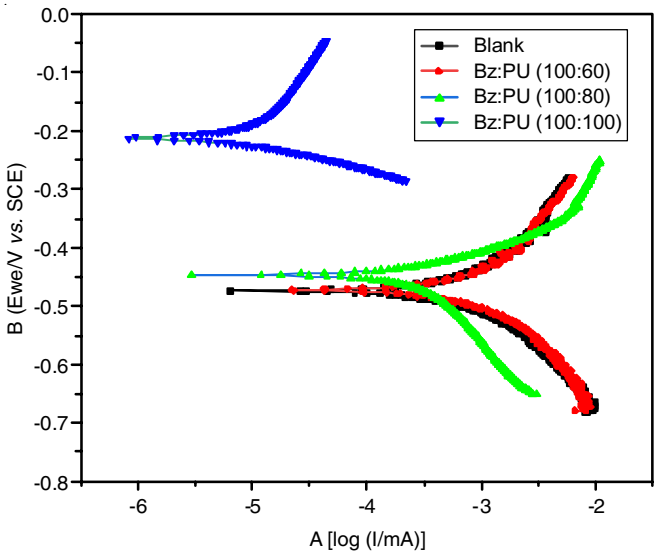

Fig. 3. Tafel polarization curves for the blank and coated VaBz-PU on mild steel

$$\text{Corrosion rate (mmpy)} = \frac{I_{corr} \times K \times EW}{\rho A} \quad (3)$$

where K = corrosion rate constant, 3272 mm $year^{-1}$, EW = equivalent weight 27.9 g, ρ = material density, 7.85 g cm^{-3} for mild steel, A = area of the sample, 1 cm^2:

$$\text{Corrosion efficiency (\%)} = \frac{I_{corr(b)} - I_{corr(c)}}{I_{corr(b)}} \times 100 \quad (4)$$

where $I_{corr(b)}$ = corrosion current values for the blank mild steel (without coating); $I_{corr(c)}$ = corrosion current values for the coated mild steel.

The free energy of adsorption (ΔG_{ads}) was calculated from eqn. 5 [36]:

$$\Delta G_{ads} = -RT \ln (55.5\ K) \quad (5)$$

where K is given by

$K = \frac{\theta}{C(1-\theta)}$, K = equilibrium constant, θ = surface coverage, C = concentration of inhibitor in mol/L, 55.5 is the concentration of water (mol/L).

From Table-2, it is depicted that by increasing the polyurethane hardener into the coating will also increase the E_{corr} values into a more positive side. The positive shift in E_{corr} shows that corrosion protection of MS surface by VaBz-PU coating was found to be better than benzoxazine coating. Generally, the diffusion rate of water into polymeric films depends upon the

TABLE-2
E_{corr}, I_{corr} AND TAFEL CONSTANT βa AND –βc VALUES OBTAINED FROM THE EXTRAPOLATION OF THE TAFEL PLOT

	I_{corr} (μA)	E_{corr} (mV)	Corrosion rate (empty)	Surface coverage (θ)	Corrosion efficiency (%)	Tafel constant		ΔG(ads) (KJ/mol)
						βa (mV/dec)	–βc (mV/dec)	
Blank	1.506	-592.048	17,513	–	–	200.7	323.5	–
100:60 (Bz:PU)	0.435	-560.253	5058	0.7111	71.11	358.7	895.8	-12.75
100:80 (Bz:PU)	0.019	-178.437	220	0.9873	98.73	390.1	117.2	-21.03
100:100 (Bz:PU)	0.005	323.131	58	0.9966	99.66	325.2	157.2	-24.06

branching and crosslinking density of the polymeric materials. The crosslinking density increases with increasing PU content in the coating; therefore, the more crosslinking density of VaBz-PU coating would reduce the porosity and enhance corrosion resistance properties. Therefore, the obtained corrosion resistance properties have been confirmed by low corrosion rates and higher corrosion efficiency up to 99.66% from the electrochemical measurements. The negative values of ΔG_{ads} indicate the spontaneous adsorption of the inhibitor on the surface of mild steel.

Electrochemical behaviours of Bz-PU coatings: The corrosion resistance of bare mild steel and the poly(Bz) coated mild steel with different content of polyurethane were further examined by EIS technique at room temperature. The recorded EIS spectra for the bare mild steel in 3.5 wt.% NaCl aqueous solutions are depicted in Fig. 4. The Nyquist plot (Fig. 4) has two time constants (i) a depressed capacitive semicircle at higher frequencies due to charge transfer in the corrosion process and (ii) an inductive loop at lower frequencies due to adsorption of a corrosion reaction intermediate [37,38]. R_s is a resistor related to the solution resistance, R_{ct} (charge transfer resistance) is a measure of electron transfer across the surface and is inversely proportional to corrosion rate and it is obtained from the diameter of the semicircles of the Nyquist plots. The inhibition efficiency of the inhibitor has been obtained from the charge transfer resistance values using eqn. 6:

$$\text{Corrosion efficiency } (\%) = \frac{R_{ct(c)} - R_{ct(b)}}{R_{ct(c)}} \times 100 \qquad (6)$$

where $R_{ct(c)}$ = charge transfer resistance with coating; $R_{ct(b)}$ = charge transfer resistance without coating.

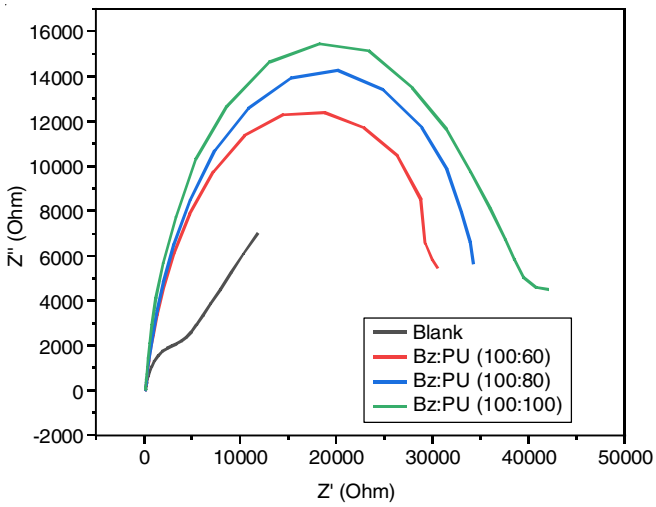

Fig. 4. Nyquist plots for the blank and coated VaBz-PU on mild steel

In Table-3, it is observed that increasing the polyurethane content on the metal surface will increase the R_{ct} from 1.0825 Ω cm^2 to 987.54 Ω cm^2 and reduce the C_{dl} value from 0.4195 F/cm^2 to 5.167 × 10^{-6} F/cm^2. A decrease in C_{dl} is due to an increase in thickness of the electronic double layer [39]. The increase in R_{ct} values is due to the formation of a protective film on the metal/solution interface [40,41]. From the R_{ct} values, it is also evident that the inhibition efficiency of VaBz-PU has increased from 91.21% to 99.89% due to the increased concentration of isocyanate (PU) content in the coating.

TABLE-3
PARAMETERS OF THE EQUIVALENT CIRCUIT IN 3.5% NaCl SOLUTIONS

Concentration of coating	R_{ct} (Ω cm^2)	C_{dl} (F/cm^2)	Inhibition efficiency (%)
Blank	1.0825	0.4195	–
100:60 (Bz:PU)	12.32	43.48 × 10^{-6}	91.21
100:80 (Bz:PU)	158.6	35.8 × 10^{-6}	99.31
100:100 (Bz:PU)	987.54	5.167 × 10^{-6}	99.89

Thermal behaviour of the coating

Thermogravimetric analysis: The thermal stability of coatings was studied by TGA analysis under a nitrogen atmosphere. The result was recorded as a weight loss of coating as a function of temperature. The values of 5 wt.% (Td5%), 30 wt.% (Td30%) loss degradation temperature and residual wt.% (char yield) at 580-600 ºC are listed in Table-4. From Fig. 5, it is observed that up to 250 ºC, the thermal stability of poly-BzPU coatings is higher than the polybenzoxazine coating. The weight loss of the poly-BzPU coatings is less than 10% whereas the polybenzoxazine coating shows a degradation of 15%. This is due to the crosslinking density of the polyurethane. The crosslinked density of the coating increases with increasing polyurethane content and has high thermal stability from 500-562 ºC. The heat-resistance index (THRI) was calculated using eqn. 7 [42,43]:

$$T_{HRI} = 0.49 \times [T_5 + 0.6 \times (T_{30} - T_5)] \qquad (7)$$

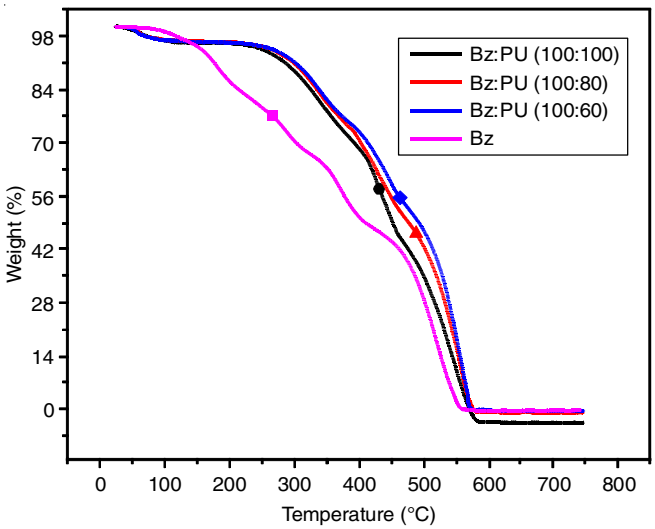

Fig. 5. TGA thermograms of cured VaBz and VaBz-PU

It is evident from Table-4 that the thermal stability of the coating increases when compared to benzoxazine coating *i.e.*, increases from 122 to 185 ºC, 181 and 179 ºC. This is due to the presence of polyurethane linkage, which enhances the crosslinking density. Due to the isocyanate unit in the coating will decrease the char yield more than VaBz [16].

DSC studies: The DSC thermogram of VaBz shows one exothermic peak at 454 ºC, which is due to the crystallization

TABLE-4
RESULTS OBTAINED FROM THERMO GRAVIMETRIC ANALYSIS OF
BENZOXAZINE, VaBz:PU ARE IN THE RATIO OF 100:60, 100:80 AND 100:100 COATINGS

Coating system	Onset temperature (°C)	Offset temperature (°C)	Td5 (°C)	Td30 (°C)	T_{HRI}
Bz	91.38	554	155.34	312.01	122.17
100:60 (Bz:PU)	201.53	570	300.91	428.81	185.04
100:80 (Bz:PU)	210.89	576	298.13	419.16	181.67
100:100 (Bz:PU)	215.09	581	292.72	414.33	179.19

temperature and the two exothermic peaks due to the melting temperatures of VaBz are 532 and 552 ºC and these are responsible for the ring opening polymerization of the VaBz (Fig. 6). The DSC thermograms of VaBz:PU show two exothermic peaks at 416, 515 ºC for Bz:PU (100:60), 416, 520 ºC for Bz:PU (100:80) and 436, 515 ºC for Bz:PU (100:100), which are due to the interaction of isocyanate moiety with VaBz through hydrogen bonding. The DSC thermograms of Bz-PU show two endothermic peaks at 458, 567 ºC for Bz:PU (100:60), 458, 574 ºC for Bz:PU (100:80) and 461, 575 ºC for Bz:PU (100:100). The first exothermic peaks at 458 and 461 °C are responsible for the ring opening due to the crosslinking ability of the polyurethane. The second peak at 567, 574 and 575 ºC occurs due to the melting of the Bz-PU. The T_g values of VaBz and Bz-PU are 252, 327, 327 and 329 vC. From Table-5, it is clearly evident that increasing PU in the coating will increase the thermal stability due to the crosslinking property of the PU. From DSC the results, it is clear that the thermal resistance of benzoxazine with polyurethane is increased when compared to benzoxazine.

SEM/EDAX studies: The scanning electron microscopy (SEM) analysis coupled with energy-dispersive X-ray analysis (EDAX) was performed in order to investigate the surface morphology of the mild steel before and after immersion in 3.5% NaCl for 1 week. The acquired results have shown that before (Fig. 7a,c,e) and after one week of immersion of the

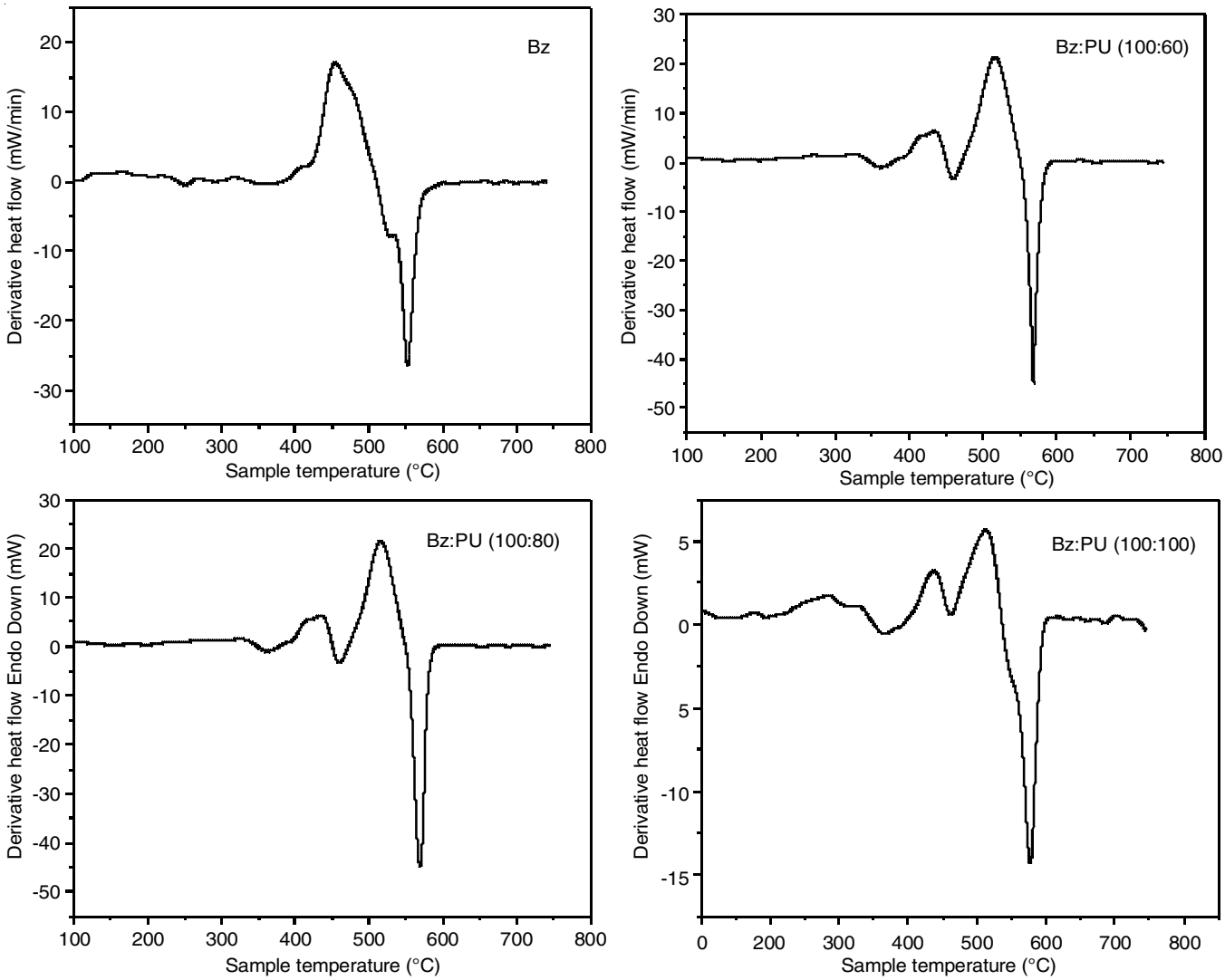

Fig. 6. DSC thermograms of cured VaBz and VaBz-PU

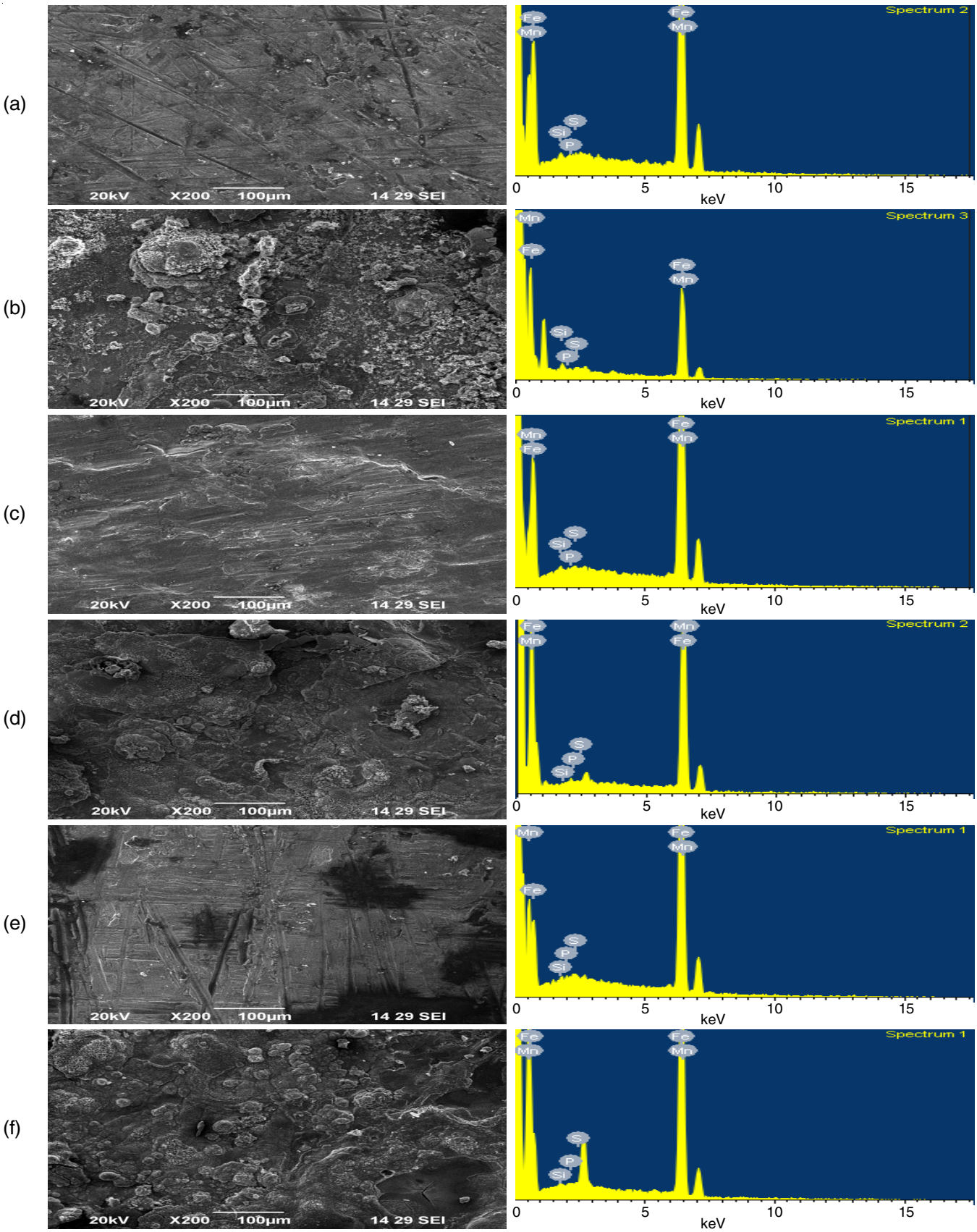

Fig. 7. SEM and EDAX analysis of mild steel before and after immersion for 1 week in 3.5% NaCl; (a) Bz-PU (100:60) before immersion in 3.5% NaCl, (b) Bz-PU (100:60) after immersion in 3.5% NaCl, (c) Bz-PU (100:80) before immersion in 3.5% NaCl, (d) Bz-PU (100:80) after immersion in 3.5% NaCl, (e) Bz-PU (100:100) before immersion in 3.5% NaCl, (f) Bz-PU (100:100) after immersion in 3.5% NaCl

TABLE-5
RESULTS OBTAINED FROM DSC OF CURED VaBz, VaBz:PU ARE IN THE RATIO OF 100:60, 100:80 AND 100:100 COATINGS

Coating system	T_g (°C)	$T_{(onset)}$ (°C)	T_{peak} (°C)	T_{peak} (°C) endo	Ref.
Bz	252	238	454	532, 552	
100:60 (Bz:PU)	360	327	416, 515	458, 567	[44-46]
100:80 (Bz:PU)	360	327	420, 515	458, 574	
100:100 (Bz:PU)	365	329	436, 515	461, 575	

coated mild steel in 3.5% NaCl (Fig. 7b,d,f) the surface of the sample was damaged and then was corroded [46,47]. However, Fig. 7d,f shows that mild steel has not been much corroded in the mild steel coated with VaBz:PU in the ratio of 100:80 and 100:100, which can be attributed to the development of a protective film on the surface of mild steel, due to the crosslinking ability of the isocyanate oxygen atom as a result the percentage of iron after immersion of NaCl is increased. The corrosion resistance on the mild steel has increased from 90.36% (for 100:60 Bz:PU) to 98.42% (100:100 Bz:PU). Hence, polyurethane along with benzoxazine protects the mild steel in 3.5% NaCl environment.

Quantum chemical calculations: The values of the quantum chemical descriptors, such as HOMO and LUMO energies (E_{HOMO} and E_{LUMO}), the gap energy (ΔEgap), chemical potential, the global hardness (η), the global softness (σ), the electrophilicity index are shown in Table-6. It is evident that HOMO density distributions are mainly localized over benzene, N and O of the oxazine ring. It indicates that these are the active centres through which these inhibitors of VaBz may be adsorbed on the metal surface by physisorption or chemisorption or from both.

Further, LUMO indicates that the substituted benzene ring along with -CHO, -OCH_3 ring moiety may involve back bonding due to the transfer of filled $4s^2$ electrons of iron metal to LUMO of benzoxazine. It should be noted here that the benzene ring of benzoxazine acts as both donor as well as acceptor centre. In general, the higher the value of HOMO, the higher would be the electron donating capacity of the inhibitor to the vacant *d*-orbital of the metal. And the lower the value of LUMO, the greater would be the electron accepting ability of the inhibitor from the filled metal orbitals. But the most important parameter is ΔE, which is the energy difference between LUMO and HOMO. Fig. 8 shows the ΔE value of VaBz is 4.395 eV and is

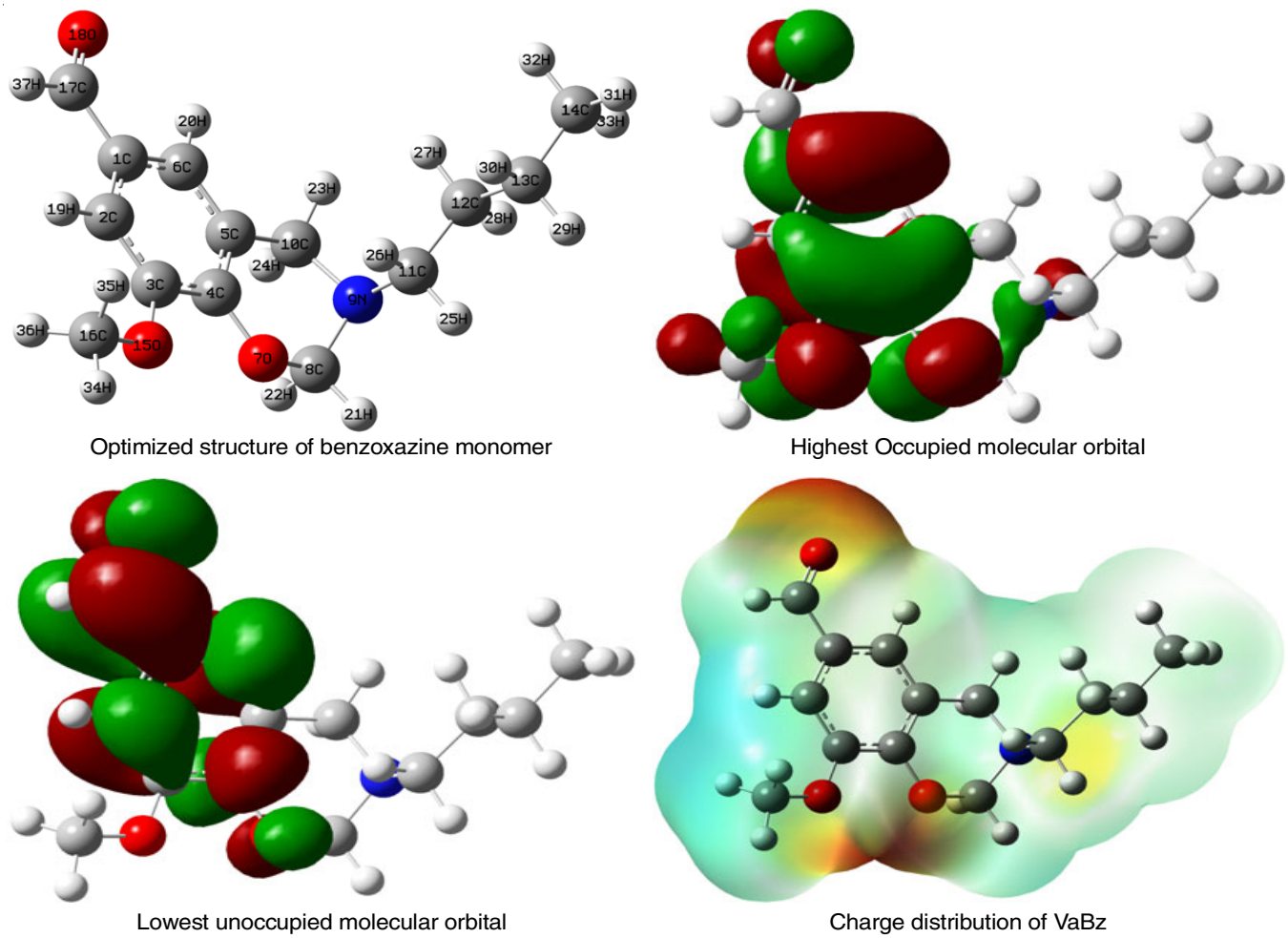

Fig. 8. Optimized structure, molecular orbital (HOMO and LUMO), charge distribution of VaBz

TABLE-6
DFT PARAMETERS

Compound name	HOMO (eV)	LUMO (eV)	Band gap (ΔE)	Chemical potential (eV)	Global hardness (eV)	Global softness (eV)	Electrophilicity index (eV)
VaBz	-5.9398	-1.5442	4.395	-3.7420	2.1977	0.2275	3.1857

very much compatible with metal-inhibitor interactions. The high global softness value 0.2275 eV and low global hardness value -3.7420 eV also supports the protection capability of the VaBz on the metal surface [48,49].

Water absorption, gel absorption and microhardness: Increasing concentration of isocyanate (PU) in the coating will increase the crosslinking ability, so this will decrease the free space due to the unavailability of the hydroxyl group and hence hydrophobicity of the monomer increased. It is evident from Fig. 9, that water absorption is decreased by increasing PU content in the coating. On the other hand, the gel absorption and microhardness increased by increasing PU content in the coating which is also evident from Figs. 10 and 11, that PU can easily form crosslinking in the presence of xylene [16].

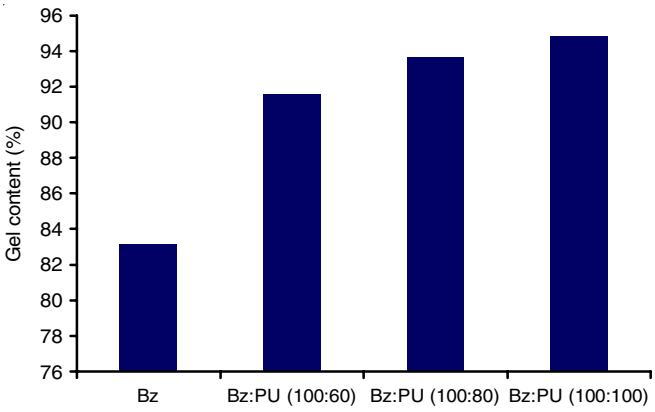

Fig. 9. Water absorption of cured VaBz and Bz-PU

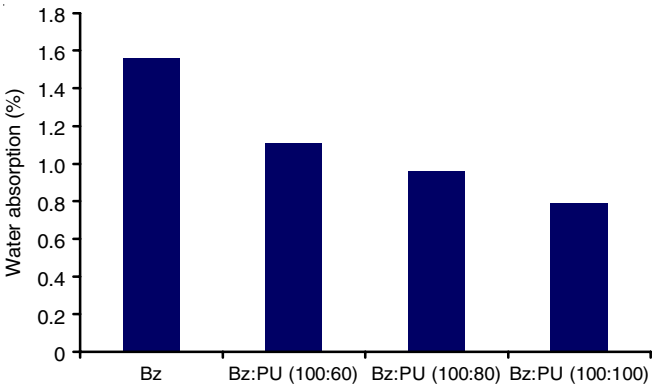

Fig. 10. Gel absorption of cured VaBz and Bz-PU

Conclusion

Vanillin-based benzoxazine has been successfully synthesized using toluene as solvent and copolymerized with different ratios of polyurethane, as well as characterized by using ^{1}H NMR, ^{13}C NMR, FTIR, UV techniques. Isocyanate in the polyurethane makes the VaBz a better inhibitor on the mild steel in 3.5% NaCl medium. Decreased corrosion rate and increased

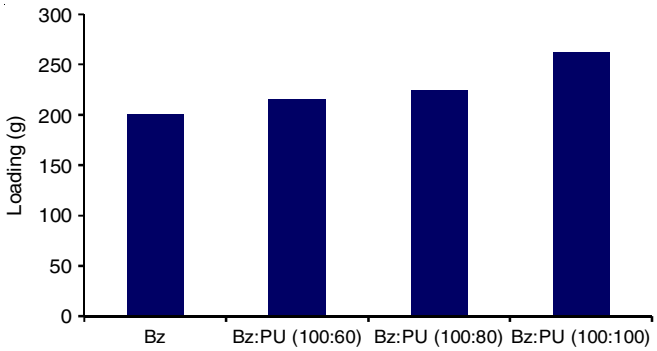

Fig. 11. Microhardness of cured VaBz and Bz-PU

inhibition efficiency due to the increasing polyurethane content in the VaBz leads the maximum inhibition efficiency up to 99% both from polarization studies as well as EIS studies. The low and negative value of ΔG_{ads} indicates that the Bz-PU is spontaneous adsorption and physically adsorbed on the mild steel. Thermal resistance (T_{HRI}) glass transition temperature (T_g) and melting temperature of the coating is also increased by the addition of polyurethane. From SEM images and EDAX studies, it is evident that the surface of the coated mild steel is protected up to 99% and less corroded in the NaCl medium. As the inter linking ability is increased by increasing polyurethane content, which elevates the microhardness, gel absorption and abates the water absorption in the Bz-PU. The DFT calculations also provide useful information about the band gap between HOMO and LUMO, global softness and global hardness is suitable for the inhibitor level. With the above information, this research proves that the benzoxazine synthesis from renewable feedstock vanillin acts as a good anticorrosive agent.

ACKNOWLEDGEMENTS

The authors express gratitude to Dr. P. Shanmugasundaram, The Head, Department of Chemistry, Thiruvalluvar Government Arts College, Rasipuram, India for the constant support and suggestions to complete this work.

CONFLICT OF INTEREST

The authors declare that there is no conflict of interests regarding the publication of this article.

REFERENCES

1. N. Haghdadi, M. Laleh, M. Moyle and S. Primig, *J. Mater. Sci.*, **56**, 64 (2021); https://doi.org/10.1007/s10853-020-05109-0
2. M. El-Sayed Sherif and H.A. Ayman, *Crystals*, **11**, 1516 (2021); https://doi.org/10.3390/cryst11121516
3. I.A. Kartsonakis, S.G. Stanciu, A.A. Matei, R. Hristu, A. Karantonis and C.A. Charitidis, *Corros. Sci.*, **112**, 289 (2016); https://doi.org/10.1016/j.corsci.2016.07.030

4. A. Dastgheib, M.M. Attar and A. Zarebidaki, *Met. Mater. Int.*, **26**, 1634 (2020); https://doi.org/10.1007/s12540-019-00432-x
5. M.A.A. Khan, O.M. Irfan, F. Djavanroodi and M. Asad, *Sustainability*, **14**, 9502 (2022); https://doi.org/10.3390/su14159502
6. G. Veselinka, B. Ivana, M. Sanja and K. Bojana, *Maced. J. Chem. Chem. Eng.*, **37**, 203 (2018).
7. L. Suman and R.S. Chaudhary, *Indian J. Chem. Technol.*, **15**, 364 (2008).
8. A.-R. El-Sayed, U. Harm, K.-M. Mangold and W. Fürbeth, *Corros. Sci.*, **55**, 339 (2012); https://doi.org/10.1016/j.corsci.2011.10.036
9. M.M. Muzakir, F.O. Nwosu and S.O. Amusat, *Port. Electrochem. Acta*, **37**, 359 (2019); https://doi.org/10.4152/pea.201906359
10. X. Li, S. Deng, X. Xie and H. Fu, *Corros. Sci.*, **87**, 15 (2014); https://doi.org/10.1016/j.corsci.2014.05.013
11. H. Ishida and D. Allen, *J. Polym. Sci., B, Polym. Phys.*, **34**, 1019 (1996); https://doi.org/10.1002/(SICI)1099-0488(19960430)34:6<1019::AID-POLB1>3.0.CO;2-T
12. H.C. Liu, W.C. Su and Y.L. Liu, *J. Mater. Chem.*, **21**, 7182 (2011); https://doi.org/10.1039/c1jm10815h
13. Y.J. Lee, S.W. Kuo, Y.C. Su, J.K. Chen, C.W. Tu and F.C. Chang, *Polymer*, **45**, 6321 (2004); https://doi.org/10.1016/j.polymer.2004.04.055
14. C. Zhou, M. Fu, H. Xie, Y. Gong, J. Chen, J. Liu and Z. Xin, *Ind. Eng. Chem. Res.*, **60**, 1675 (2021); https://doi.org/10.1021/acs.iecr.0c05903
15. T. Periyasamy, S.P. Asrafali, S. Muthusamy and S.-C. Kim, *New J. Chem.*, **40**, 9313 (2016); https://doi.org/10.1039/C6NJ02242A
16. G.A. Phalak, D.M. Patil and S.T. Mhaske, *Eur. Polym. J.*, **88**, 93 (2017); https://doi.org/10.1016/j.eurpolymj.2016.12.030
17. D.M. Patil, G.A. Phalak and S.T. Mhaske, *Prog. Org. Coat.*, **105**, 18 (2017); https://doi.org/10.1016/j.porgcoat.2016.10.027
18. M. Fache, B. Boutevin and S. Caillol, *Eur. Polym. J.*, **68**, 488 (2015); https://doi.org/10.1016/j.eurpolymj.2015.03.050
19. A. Van, K. Chiou and H. Ishida, *Polymer*, **55**, 1443 (2014); https://doi.org/10.1016/j.polymer.2014.01.041
20. N.K. Sini, J. Bijwe and I.K. Varma, *Polym. Degrad. Stab.*, **109**, 270 (2014); https://doi.org/10.1016/j.polymdegradstab.2014.07.015
21. N.K. Sini, J. Bijwe and I.K. Varma, *J. Polym. Sci. A Polym. Chem.*, **52**, 7 (2014); https://doi.org/10.1002/pola.26981
22. C. Chen, Y. Cao, X. Lu, X. Li, H. Yao and Z. Xin, *Colloids Surf. A Physicochem. Eng. Asp.*, **609**, 125605 (2021); https://doi.org/10.1016/j.colsurfa.2020.125605
23. M.S. Mahajan, P.P. Mahulikar and V.V. Gite, *Prog. Org. Coat.*, **148**, 105826 (2020); https://doi.org/10.1016/j.porgcoat.2020.105826
24. R.L. Quirino, T.F. Garrison and M.R. Kessler, *Green Chem.*, **16**, 1700 (2014); https://doi.org/10.1039/C3GC41811A
25. G. Wu, X. He, L. Xu, H. Zhang and Y. Yan, *RSC Adv.*, **5**, 27097 (2015); https://doi.org/10.1039/C5RA02912K
26. A.S. More, B. Gadenne, C. Alfos and H. Cramail, *Polym. Chem.*, **3**, 1594 (2012); https://doi.org/10.1039/c2py20123b
27. T.J. Nelson, B. Masaki, Z. Morseth and D.C. Webster, *J. Coat. Technol. Res.*, **10**, 757 (2013); https://doi.org/10.1007/s11998-013-9524-0
28. C. Zhang, S.A. Madbouly and M.R. Kessler, *ACS Appl. Mater. Interfaces*, **7**, 1226 (2015); https://doi.org/10.1021/am5071333
29. P. Thirukumaran, P.A. Shakila, M. Sarojadevi and C.K. Seong, *New J. Chem.*, **43**, 8816 (2020); https://doi.org/10.1039/C9NJ90071C
30. A. Trejo-Machin, A. Adjaoud, L. Puchot, R. Dieden and P. Verge, *Eur. Polym. J.*, **124**, 109468 (2020); https://doi.org/10.1016/j.eurpolymj.2019.109468
31. X. Ning and H. Ishida, *J. Polym. Sci. A Polym. Chem.*, **32**, 1121 (1994); https://doi.org/10.1002/pola.1994.080320614
32. J.A. Macko and H. Ishida, *Polymer*, **42**, 6371 (2001); https://doi.org/10.1016/S0032-3861(01)00055-6
33. R.-C. Lin and S.-W. Kuo, *RSC Adv.*, **8**, 13592 (2018); https://doi.org/10.1039/C8RA00506K
34. C. Zhou, X. Lu, Z. Xin and Y. Zhang, *J. Coat. Technol. Res.*, **13**, 63 (2016); https://doi.org/10.1007/s11998-015-9722-z
35. H. Wei, D. Ding, S. Wei and Z. Guo, *J. Mater. Chem. A Mater. Energy Sustain.*, **1**, 10805 (2013); https://doi.org/10.1039/c3ta11966a
36. P. Selvakumar, K.B. Balanaga and C. Thangavelu, *J. Adv. Chem.*, **6**, 897 (2013).
37. Z. Tao, S. Zhang, W. Li and B. Hou, *Corros. Sci.*, **51**, 2588 (2009); https://doi.org/10.1016/j.corsci.2009.06.042
38. P.C. Okafor, X. Liu and Y.G. Zheng, *Corros. Sci.*, **51**, 761 (2009); https://doi.org/10.1016/j.corsci.2009.01.017
39. M.G. Hosseini, M. Ehteshamzadeh and T. Shahrabi, *Electrochim. Acta*, **52**, 3680 (2007); https://doi.org/10.1016/j.electacta.2006.10.041
40. S. Muralidharan, K.L.N. Phani, S. Pitchumani, S. Ravichandran and S.V.K. Iyer, *J. Electrochem. Soc.*, **142**, 1478 (1995); https://doi.org/10.1149/1.2048599
41. F. Bentiss, M. Traisnel and M. Lagrenee, *Corros. Sci.*, **42**, 127 (2000); https://doi.org/10.1016/S0010-938X(99)00049-9
42. X. Yang, S. Fan, Y. Li, Y. Guo, Y. Li, K. Ruan, S. Zhang, J. Zhang, J. Kong and J. Gu, *Composites Part A*, **128**, 105670 (2020); https://doi.org/10.1016/j.compositesa.2019.105670
43. P. Song, H. Wang, L. Wang, X. Liu, Y. Zhang, J. Zhang, J. Kong and J. Gu, *Sustain. Mater. Technol.,* **24** e00153 (2020); https://doi.org/10.1016/j.susmat.2020.e00153
44. S. Sriharshitha, K. Krishnadevi, S. Devaraju, V. Srinivasadesikan and S.-L. Lee, *ACS Omega*, **5**, 33178 (2020); https://doi.org/10.1021/acsomega.0c04840
45. P. Sharma, P. Dutta and L. Nebhani, *Polymer*, **184**, 121905 (2019); https://doi.org/10.1016/j.polymer.2019.121905
46. P. Sharma and L. Nebhani, *Polymer*, **199**, 122549 (2020); https://doi.org/10.1016/j.polymer.2020.122549
47. A. Ouass, M. Galai, M. Ouakki, E. Ech-Chihbi, L. Kadiri, R. Hsissou, Y. Essaadaoui, A. Berisha, M. Cherkaoui, A. Lebkiri and E.H. Rifi, *J. Appl. Electrochem.*, **51**, 1009 (2021); https://doi.org/10.1007/s10800-021-01556-y
48. J. Fang and J. Li, *J. Mol. Struct. THEOCHEM*, **593**, 179 (2002); https://doi.org/10.1016/S0166-1280(02)00316-0
49. D.K. Singh, E.E. Ebenso, M.K. Singh, D. Behera, G. Udayabhanu and R.P. John, *J. Mol. Liq.*, **250**, 88 (2018); https://doi.org/10.1016/j.molliq.2017.11.132